Measurement of the single top quark production cross section and |V tb | in 1.96 TeV pp collisions with missing transverse energy and jets and final CDF combination

Journal Article

Author(s):
CDF Collaboration; Aaltonen, T.; Casal, Bruno; Wallny, Rainer; et al.

Measurement of the single top quark production cross section and $|V_{tb}|$ in 1.96 TeV $p\bar{p}$ collisions with missing transverse energy and jets and final CDF combination

T. Aaltonen,[21] S. Amerio,[39a,39b] D. Amidei,[31] A. Anastassov,[15,v] A. Annovi,[17] J. Antos,[12] G. Apollinari,[15] J. A. Appel,[15]
T. Arisawa,[52] A. Artikov,[13] J. Asaadi,[47] W. Ashmanskas,[15] B. Auerbach,[2] A. Aurisano,[47] F. Azfar,[38] W. Badgett,[15] T. Bae,[25]
A. Barbaro-Galtieri,[26] V. E. Barnes,[43] B. A. Barnett,[23] P. Barria,[41a,41c] P. Bartos,[12] M. Bauce,[39a,39b] F. Bedeschi,[41a]
S. Behari,[15] G. Bellettini,[41a,41b] J. Bellinger,[54] D. Benjamin,[14] A. Beretvas,[15] A. Bhatti,[45] K. R. Bland,[5] B. Blumenfeld,[23]
A. Bocci,[14] A. Bodek,[44] D. Bortoletto,[43] J. Boudreau,[42] A. Boveia,[11] L. Brigliadori,[6a,6b] C. Bromberg,[32] E. Brucken,[21]
J. Budagov,[13] H. S. Budd,[44] K. Burkett,[15] G. Busetto,[39a,39b] P. Bussey,[19] P. Butti,[41a,41b] A. Buzatu,[19] A. Calamba,[10]
S. Camarda,[4] M. Campanelli,[28] F. Canelli,[11,cc] B. Carls,[22] D. Carlsmith,[54] R. Carosi,[41a] S. Carrillo,[16,l] B. Casal,[9,j]
M. Casarsa,[48a] A. Castro,[6a,6b] P. Catastini,[20] D. Cauz,[48a,48b,48c] V. Cavaliere,[22] A. Cerri,[26,e] L. Cerrito,[28,q] Y. C. Chen,[1]
M. Chertok,[7] G. Chiarelli,[41a] G. Chlachidze,[15] K. Cho,[25] D. Chokheli,[13] A. Clark,[18] C. Clarke,[53] M. E. Convery,[15]
J. Conway,[7] M. Corbo,[15,y] M. Cordelli,[17] C. A. Cox,[7] D. J. Cox,[7] M. Cremonesi,[41a] D. Cruz,[47] J. Cuevas,[9,x] R. Culbertson,[15]
N. d'Ascenzo,[15,u] M. Datta,[15,ff] P. de Barbaro,[44] L. Demortier,[45] M. Deninno,[6a] M. D'Errico,[39a,39b] F. Devoto,[21]
A. Di Canto,[41a,41b] B. Di Ruzza,[15,p] J. R. Dittmann,[5] S. Donati,[41a,41b] M. D'Onofrio,[27] M. Dorigo,[48a,48d] A. Driutti,[48a,48b,48c]
K. Ebina,[52] R. Edgar,[31] A. Elagin,[47] R. Erbacher,[7] S. Errede,[22] B. Esham,[22] S. Farrington,[38] J. P. Fernández Ramos,[29]
R. Field,[16] G. Flanagan,[15,s] R. Forrest,[7] M. Franklin,[20] J. C. Freeman,[15] H. Frisch,[11] Y. Funakoshi,[52] C. Galloni,[41a,41b]
A. F. Garfinkel,[43] P. Garosi,[41a,41c] H. Gerberich,[22] E. Gerchtein,[15] S. Giagu,[46a] V. Giakoumopoulou,[3] K. Gibson,[42]
C. M. Ginsburg,[15] N. Giokaris,[3] P. Giromini,[17] V. Glagolev,[13] D. Glenzinski,[15] M. Gold,[34] D. Goldin,[47] A. Golossanov,[15]
G. Gomez,[9] G. Gomez-Ceballos,[30] M. Goncharov,[30] O. González López,[29] I. Gorelov,[34] A. T. Goshaw,[14] K. Goulianos,[45]
E. Gramellini,[6a] C. Grosso-Pilcher,[11] R. C. Group,[51,15] J. Guimaraes da Costa,[20] S. R. Hahn,[15] J. Y. Han,[44] F. Happacher,[17]
K. Hara,[49] M. Hare,[50] R. F. Harr,[53] T. Harrington-Taber,[15,m] K. Hatakeyama,[5] C. Hays,[38] J. Heinrich,[40] M. Herndon,[54]
A. Hocker,[15] Z. Hong,[47] W. Hopkins,[15,f] S. Hou,[1] R. E. Hughes,[35] U. Husemann,[55] M. Hussein,[32,aa] J. Huston,[32]
G. Introzzi,[41a,41e,41f] M. Iori,[46a,46b] A. Ivanov,[7,o] E. James,[15] D. Jang,[10] B. Jayatilaka,[15] E. J. Jeon,[25] S. Jindariani,[15]
M. Jones,[43] K. K. Joo,[25] S. Y. Jun,[10] T. R. Junk,[15] M. Kambeitz,[24] T. Kamon,[25,47] P. E. Karchin,[53] A. Kasmi,[5] Y. Kato,[37,n]
W. Ketchum,[11,gg] J. Keung,[40] B. Kilminster,[15,cc] D. H. Kim,[25] H. S. Kim,[25] J. E. Kim,[25] M. J. Kim,[17] S. H. Kim,[49]
S. B. Kim,[25] Y. J. Kim,[25] Y. K. Kim,[11] N. Kimura,[52] M. Kirby,[15] K. Knoepfel,[15] K. Kondo,[52,*] D. J. Kong,[25] J. Konigsberg,[16]
A. V. Kotwal,[14] M. Kreps,[24] J. Kroll,[40] M. Kruse,[14] T. Kuhr,[24] M. Kurata,[49] A. T. Laasanen,[43] S. Lammel,[15] M. Lancaster,[28]
K. Lannon,[35,w] G. Latino,[41a,41c] H. S. Lee,[25] J. S. Lee,[25] S. Leo,[41a] S. Leone,[41a] J. D. Lewis,[15] A. Limosani,[14,r] E. Lipeles,[40]
A. Lister,[18,a] H. Liu,[51] Q. Liu,[43] T. Liu,[15] S. Lockwitz,[55] A. Loginov,[55] D. Lucchesi,[39a,39b] A. Lucà,[17] J. Lueck,[24] P. Lujan,[26]
P. Lukens,[15] G. Lungu,[45] J. Lys,[26] R. Lysak,[12,d] R. Madrak,[15] P. Maestro,[41a,41c] S. Malik,[45] G. Manca,[27,b]
A. Manousakis-Katsikakis,[3] L. Marchese,[6a,hh] F. Margaroli,[46a] P. Marino,[41a,41d] K. Matera,[22] M. E. Mattson,[53]
A. Mazzacane,[15] P. Mazzanti,[6a] R. McNulty,[27,i] A. Mehta,[27] P. Mehtala,[21] C. Mesropian,[45] T. Miao,[15] D. Mietlicki,[31]
A. Mitra,[1] H. Miyake,[49] S. Moed,[15] N. Moggi,[6a] C. S. Moon,[15,y] R. Moore,[15,dd,ee] M. J. Morello,[41a,41d] A. Mukherjee,[15]
Th. Muller,[24] P. Murat,[15] M. Mussini,[6a,6b] J. Nachtman,[15,m] Y. Nagai,[49] J. Naganoma,[52] I. Nakano,[36] A. Napier,[50] J. Nett,[47]
C. Neu,[51] T. Nigmanov,[42] L. Nodulman,[2] S. Y. Noh,[25] O. Norniella,[22] L. Oakes,[38] S. H. Oh,[14] Y. D. Oh,[25] I. Oksuzian,[51]
T. Okusawa,[37] R. Orava,[21] L. Ortolan,[4] C. Pagliarone,[48a] E. Palencia,[9,e] P. Palni,[34] V. Papadimitriou,[15] W. Parker,[54]
G. Pauletta,[48a,48b,48c] M. Paulini,[10] C. Paus,[30] T. J. Phillips,[14] E. Pianori,[40] J. Pilot,[7] K. Pitts,[22] C. Plager,[8] L. Pondrom,[54]
S. Poprocki,[15,f] K. Potamianos,[26] A. Pranko,[26] F. Prokoshin,[13,z] F. Ptohos,[17,g] G. Punzi,[41a,41b] I. Redondo Fernández,[29]
P. Renton,[38] M. Rescigno,[46a] F. Rimondi,[6a,*] L. Ristori,[41a,15] A. Robson,[19] T. Rodriguez,[40] S. Rolli,[50,h] M. Ronzani,[41a,41b]
R. Roser,[15] J. L. Rosner,[11] F. Ruffini,[41a,41c] A. Ruiz,[9] J. Russ,[10] V. Rusu,[15] W. K. Sakumoto,[44] Y. Sakurai,[52] L. Santi,[48a,48b,48c]
K. Sato,[49] V. Saveliev,[15,u] A. Savoy-Navarro,[15,y] P. Schlabach,[15] E. E. Schmidt,[15] T. Schwarz,[31] L. Scodellaro,[9] F. Scuri,[41a]
S. Seidel,[34] Y. Seiya,[37] A. Semenov,[13] F. Sforza,[41a,41b] S. Z. Shalhout,[7] T. Shears,[27] P. F. Shepard,[42] M. Shimojima,[49,t]
M. Shochet,[11] I. Shreyber-Tecker,[33] A. Simonenko,[13] K. Sliwa,[50] J. R. Smith,[7] F. D. Snider,[15] H. Song,[42] V. Sorin,[4] R. St.
Denis,[19,*] M. Stancari,[15] D. Stentz,[15,v] J. Strologas,[34] Y. Sudo,[49] A. Sukhanov,[15] I. Suslov,[13] K. Takemasa,[49] Y. Takeuchi,[49]
J. Tang,[11] M. Tecchio,[31] P. K. Teng,[1] J. Thom,[15,f] E. Thomson,[40] V. Thukral,[47] D. Toback,[47] D. Tobell,[47] K. Tollefson,[32]
T. Tomura,[49] D. Tonelli,[15,e] S. Torre,[17] D. Torretta,[15] P. Totaro,[39a] M. Trovato,[41a,41d] F. Ukegawa,[49] S. Uozumi,[25]
F. Vázquez,[16,l] G. Velev,[15] C. Vellidis,[15] C. Vernieri,[41a,41d] M. Vidal,[43] R. Vilar,[9] J. Vizán,[9,bb] M. Vogel,[34] G. Volpi,[17]
P. Wagner,[40] R. Wallny,[15,j] S. M. Wang,[1] D. Waters,[28] W. C. Wester III,[15] D. Whiteson,[40,c] A. B. Wicklund,[2] S. Wilbur,[7]
H. H. Williams,[40] J. S. Wilson,[31] P. Wilson,[15] B. L. Winer,[35] P. Wittich,[15,f] S. Wolbers,[15] H. Wolfe,[35] T. Wright,[31] X. Wu,[18]
Z. Wu,[5] K. Yamamoto,[37] D. Yamato,[37] T. Yang,[15] U. K. Yang,[25] Y. C. Yang,[25] W.-M. Yao,[26] G. P. Yeh,[15] K. Yi,[15,m] J. Yoh,[15]
K. Yorita,[52] T. Yoshida,[37,k] G. B. Yu,[14] I. Yu,[25] A. M. Zanetti,[48a] Y. Zeng,[14] C. Zhou,[14] and S. Zucchelli[6a,6b]

(CDF Collaboration)

[1]Institute of Physics, Academia Sinica, Taipei, Taiwan 11529,
Republic of China

[2]Argonne National Laboratory, Argonne, Illinois 60439, USA

[3]University of Athens, 157 71 Athens, Greece

[4]Institut de Fisica d'Altes Energies, ICREA, Universitat Autonoma de Barcelona,
E-08193, Bellaterra (Barcelona), Spain

[5]Baylor University, Waco, Texas 76798, USA

[6a]Istituto Nazionale di Fisica Nucleare Bologna, I-40127 Bologna, Italy

[6b]University of Bologna, I-40127 Bologna, Italy

[7]University of California, Davis, Davis, California 95616, USA

[8]University of California, Los Angeles, Los Angeles, California 90024, USA

[9]Instituto de Fisica de Cantabria, CSIC-University of Cantabria, 39005 Santander, Spain

[10]Carnegie Mellon University, Pittsburgh, Pennsylvania 15213, USA

[11]Enrico Fermi Institute, University of Chicago, Chicago, Illinois 60637, USA

[12]Comenius University, 842 48 Bratislava, Slovakia; Institute of Experimental Physics,
040 01 Kosice, Slovakia

[13]Joint Institute for Nuclear Research, RU-141980 Dubna, Russia

[14]Duke University, Durham, North Carolina 27708, USA

[15]Fermi National Accelerator Laboratory, Batavia, Illinois 60510, USA

[16]University of Florida, Gainesville, Florida 32611, USA

[17]Laboratori Nazionali di Frascati, Istituto Nazionale di Fisica Nucleare, I-00044 Frascati, Italy

[18]University of Geneva, CH-1211 Geneva 4, Switzerland

[19]Glasgow University, Glasgow G12 8QQ, United Kingdom

[20]Harvard University, Cambridge, Massachusetts 02138, USA

[21]Division of High Energy Physics, Department of Physics, University of Helsinki, FIN-00014, Helsinki,
Finland; Helsinki Institute of Physics, FIN-00014, Helsinki, Finland

[22]University of Illinois, Urbana, Illinois 61801, USA

[23]The Johns Hopkins University, Baltimore, Maryland 21218, USA

[24]Institut für Experimentelle Kernphysik, Karlsruhe Institute of Technology, D-76131 Karlsruhe, Germany

[25]Center for High Energy Physics: Kyungpook National University, Daegu 702-701, Korea;
Seoul National University, Seoul 151-742, Korea; Sungkyunkwan University, Suwon 440-746, Korea;
Korea Institute of Science and Technology Information, Daejeon 305-806, Korea;
Chonnam National University, Gwangju 500-757, Korea; Chonbuk National University,
Jeonju 561-756, Korea;
Ewha Womans University, Seoul, 120-750, Korea

[26]Ernest Orlando Lawrence Berkeley National Laboratory, Berkeley, California 94720, USA

[27]University of Liverpool, Liverpool L69 7ZE, United Kingdom

[28]University College London, London WC1E 6BT, United Kingdom

[29]Centro de Investigaciones Energeticas Medioambientales y Tecnologicas, E-28040 Madrid, Spain

[30]Massachusetts Institute of Technology, Cambridge, Massachusetts 02139, USA

[31]University of Michigan, Ann Arbor, Michigan 48109, USA

[32]Michigan State University, East Lansing, Michigan 48824, USA

[33]Institution for Theoretical and Experimental Physics, ITEP, Moscow 117259, Russia

[34]University of New Mexico, Albuquerque, New Mexico 87131, USA

[35]The Ohio State University, Columbus, Ohio 43210, USA

[36]Okayama University, Okayama 700-8530, Japan

[37]Osaka City University, Osaka 558-8585, Japan

[38]University of Oxford, Oxford OX1 3RH, United Kingdom

[39a]Istituto Nazionale di Fisica Nucleare, Sezione di Padova, I-35131 Padova, Italy

[39b]University of Padova, I-35131 Padova, Italy

[40]University of Pennsylvania, Philadelphia, Pennsylvania 19104, USA

[41a]Istituto Nazionale di Fisica Nucleare Pisa, I-56127 Pisa, Italy

[41b]University of Pisa, I-56127 Pisa, Italy

[41c]University of Siena, I-56127 Pisa, Italy

[41d]Scuola Normale Superiore, I-56127 Pisa, Italy

[41e]INFN Pavia, I-27100 Pavia, Italy

[41f]University of Pavia, I-27100 Pavia, Italy

[42]University of Pittsburgh, Pittsburgh, Pennsylvania 15260, USA

[43]Purdue University, West Lafayette, Indiana 47907, USA

[44]University of Rochester, Rochester, New York 14627, USA

[45]*The Rockefeller University, New York, New York 10065, USA*
[46a]*Istituto Nazionale di Fisica Nucleare, Sezione di Roma 1, I-00185 Roma, Italy*
[46b]*Sapienza Università di Roma, I-00185 Roma, Italy*
[47]*Mitchell Institute for Fundamental Physics and Astronomy, Texas A&M University,
College Station, Texas 77843, USA*
[48a]*Istituto Nazionale di Fisica Nucleare Trieste, I-33100 Udine, Italy*
[48b]*Gruppo Collegato di Udine, I-33100 Udine, Italy*
[48c]*University of Udine, I-33100 Udine, Italy*
[48d]*University of Trieste, I-34127 Trieste, Italy*
[49]*University of Tsukuba, Tsukuba, Ibaraki 305, Japan*
[50]*Tufts University, Medford, Massachusetts 02155, USA*
[51]*University of Virginia, Charlottesville, Virginia 22906, USA*
[52]*Waseda University, Tokyo 169, Japan*
[53]*Wayne State University, Detroit, Michigan 48201, USA*
[54]*University of Wisconsin, Madison, Wisconsin 53706, USA*
[55]*Yale University, New Haven, Connecticut 06520, USA*

An updated measurement of the single top quark production cross section is presented using the full data set collected by the Collider Detector at Fermilab (CDF), corresponding to 9.5 fb^{-1} of integrated luminosity from proton-antiproton collisions at 1.96 TeV center-of-mass energy. The events selected contain an imbalance in the total transverse momentum, jets identified as containing b quarks, and no identified leptons. The sum of the s- and t-channel single top quark cross sections is measured to be $3.53^{+1.25}_{-1.16}$ pb and a lower limit on the magnitude of the top-to-bottom quark coupling, $|V_{tb}|$ of 0.63, is

[*]Deceased.
[a]University of British Columbia, Vancouver, BC V6T 1Z1, Canada.
[b]Istituto Nazionale di Fisica Nucleare, Sezione di Cagliari, 09042 Monserrato (Cagliari), Italy.
[c]University of California Irvine, Irvine, CA 92697, USA.
[d]Institute of Physics, Academy of Sciences of the Czech Republic, 182 21, Czech Republic.
[e]CERN, CH-1211 Geneva, Switzerland.
[f]Cornell University, Ithaca, NY 14853, USA.
[g]University of Cyprus, Nicosia CY-1678, Cyprus.
[h]Office of Science, U.S. Department of Energy, Washington, DC 20585, USA.
[i]University College Dublin, Dublin 4, Ireland.
[j]ETH, 8092 Zürich, Switzerland.
[k]University of Fukui, Fukui City, Fukui Prefecture, Japan 910-0017.
[l]Universidad Iberoamericana, Lomas de Santa Fe, México, C.P. 01219, Distrito Federal.
[m]University of Iowa, Iowa City, IA 52242, USA.
[n]Kinki University, Higashi-Osaka City, Japan 577-8502.
[o]Kansas State University, Manhattan, KS 66506, USA.
[p]Brookhaven National Laboratory, Upton, NY 11973, USA.
[q]Queen Mary, University of London, London, E1 4NS, United Kingdom.
[r]University of Melbourne, Victoria 3010, Australia.
[s]Muons, Inc., Batavia, IL 60510, USA.
[t]Nagasaki Institute of Applied Science, Nagasaki 851-0193, Japan.
[u]National Research Nuclear University, Moscow 115409, Russia.
[v]Northwestern University, Evanston, IL 60208, USA.
[w]University of Notre Dame, Notre Dame, IN 46556, USA.
[x]Universidad de Oviedo, E-33007 Oviedo, Spain.
[y]CNRS-IN2P3, Paris, F-75205 France.
[z]Universidad Tecnica Federico Santa Maria, 110v Valparaiso, Chile.
[aa]The University of Jordan, Amman 11942, Jordan.
[bb]Universite catholique de Louvain, 1348 Louvain-La-Neuve, Belgium.
[cc]University of Zürich, 8006 Zürich, Switzerland.
[dd]Massachusetts General Hospital, Boston, MA 02114 USA.
[ee]Harvard Medical School, Boston, MA 02114 USA.
[ff]Hampton University, Hampton, VA 23668, USA.
[gg]Los Alamos National Laboratory, Los Alamos, NM 87544, USA.
[hh]Università degli Studi di Napoli Federico I, I-80138 Napoli, Italy.

obtained at the 95% credibility level. These measurements are combined with previously reported CDF results obtained from events with an imbalance in total transverse momentum, jets identified as originating from b quarks, and one identified lepton. The combined cross section is measured to be $3.02^{+0.49}_{-0.48}$ pb and a lower limit on $|V_{tb}|$ of 0.84 is obtained at the 95% credibility level.

The observation of single top quark production [1], first achieved in proton-antiproton collisions, was remarkable, given the small production cross section and the copious backgrounds from processes containing heavy bosons. Since the production amplitude is proportional to the Wtb coupling, the measurement of the single top quark production cross section offers a way to determine directly the magnitude of the Cabibbo-Kobayashi-Maskawa (CKM) [2] matrix element V_{tb}. This is the only way to measure V_{tb} without assuming the unitarity of the CKM matrix. Checking the unitarity of the CKM matrix is among the most powerful approaches to test for the presence of broad classes of particles or interactions not described by the standard model (SM). These couplings have been the subject of intense experimental activity in the past three decades.

For single top quark production, a $t\bar{b}$ pair is produced by exchanging a virtual W^+ boson in either the s or the t channel. The top quark subsequently decays to a W^+ boson and a b quark, and fragmentation and hadronization of the b and $\bar{b}$ quarks result in two jets that can be reconstructed in the detector. For the t-channel process, jets tend to be more boosted along the proton-antiproton beam axis than those originating from the s-channel process. Thus, some of the t-channel jets especially are emitted in regions that are not instrumented and therefore escape the detector acceptance. Examples of SM single top quark production processes dominating at the Tevatron are shown in Fig. 1.

Excluding the contribution from the tW production mode, which is expected to be negligible in the final state considered in this paper [3], the SM prediction for the combined s- and t-channel single top quark production cross section σ_{SM}^{s+t} is 3.15 ± 0.36 pb, which has been calculated including next-to-next-to-leading order corrections [4,5]. The primary sensitivity to measuring this quantity is usually obtained from events in which the W boson from the $t \rightarrow W^+ b$ process [6] decays leptonically to a charged lepton ℓ (where ℓ represents either an electron e or muon μ) and an antineutrino, with a pair of jets, one of which is "b-tagged" or identified as likely containing one or more weakly-decaying B hadrons. This sample of events (hereafter the "$\ell\nu b\bar{b}$" sample) provides a distinctive signature against backgrounds produced by the strong interaction (QCD multijet or "MJ" background) which contain multiple jets, but no leptons.

A complementary approach consists of using final states that contain two or three jets and significant imbalance in the total transverse energy $\not{E}_T$ [7], and no reconstructed lepton. This event topology occurs when the lepton from the W boson decay is not identified due to acceptance or reconstruction effects, and the unmeasured neutrino carries a large transverse momentum. Although MJ events comprise the dominant background in this final state (hereafter the "$\not{E}_T b\bar{b}$" analysis or sample), the requirement of significant $\not{E}_T$ greatly suppresses such background. In addition, this search has sensitivity to events in which the W boson decays via $W^- \rightarrow \tau^- \bar{\nu}_\tau$, and the τ^- decays hadronically, resulting in a reconstructed jet signature.

The first measurement at the Collider Detector at Fermilab (CDF) of single top quark production in the $\not{E}_T b\bar{b}$ final state was performed with a proton-antiproton collision data set corresponding to an integrated luminosity of 2.1 fb^{-1} [8]. This paper presents an updated measurement using the full CDF data set (9.5 fb^{-1}). All the techniques developed in the search for s-channel single top quark production in the $\not{E}_T b\bar{b}$ sample [9] are exploited in this update. Important aspects of the analysis methodology are described. The results of this analysis and those of the most recent $\ell\nu b\bar{b}$ analysis [10] are then combined to obtain a more precise measurement of the single top quark cross section and to place a lower limit on $|V_{tb}|$.

The CDF II detector is a multipurpose particle detector [11]. It is comprised of an inner silicon vertex detector, a 96-layer drift chamber spectrometer used for reconstructing charged-particle trajectories (tracks), and a calorimeter that is divided radially into electromagnetic and hadronic compartments, which are constructed of projective towers that cover pseudorapidities of up to $|\eta| < 3.6$ [12]. Drift chambers located outside the hadronic calorimeter are used for muon identification.

Jets are formed by clustering calorimeter energy deposits within a cone which subtends $\Delta R \equiv \sqrt{(\Delta\eta)^2 + (\Delta\phi)^2} = 0.4$. Lepton candidates with large
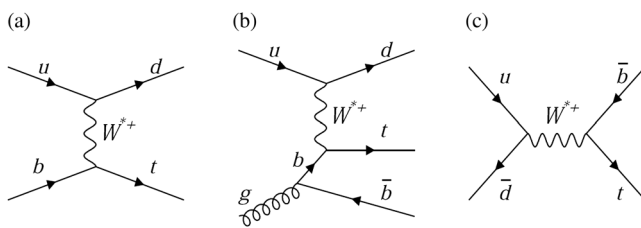

FIG. 1. Feynman diagrams for electroweak single top quark production: (a) leading-order t-channel, (b) next-to-leading-order t-channel, and (c) leading-order s-channel.

transverse momentum are identified by associating tracks with signatures in the appropriate detectors: energy deposits in the electromagnetic calorimeters for electrons, and muon-detector track segments for muons.

Events are selected in which the calorimeter missing transverse energy $\not{E}_T(\mathrm{cal})$ satisfies a minimum online selection (trigger) threshold of at least 45 GeV , or 35 GeV if at least two jets are present. The efficiency associated with this selection is obtained from data and is applied to the Monte Carlo simulated samples. A multivariate algorithm is used to parametrize the trigger efficiency as a function of several kinematic and angular variables of the event [13]. In the offline analysis, events are accepted if the reconstructed missing transverse energy, after corrections to jet energies to account for detector defects and jet size fluctuations in the calorimeters, is at least 35 GeV. Measured jet energies are corrected to account for nonuniformities in calorimeter response, energy lost outside the jet cone, and underlying event dynamics [14]. The jet energy scale and resolution, as well as the $\not{E}_T$ resolution, are further improved by incorporating corrections based on charged-particle momentum measurements [15].

Each event is required to have two jets with transverse energies $E_T^{j_1}$ and $E_T^{j_2}$ that satisfy $25 < E_T^{j_1} < 200$ GeV and $20 < E_T^{j_2} < 120$ GeV, respectively. Additionally, both of these jets are required to be reconstructed within the silicon detector acceptance, corresponding to a pseudorapidity requirements of $|\eta| < 2$, and one of the jets must satisfy $|\eta| < 0.9$. Events with three jets are considered if the third jet satisfies $15 < E_T^{j_3} < 100$ GeV and $|\eta| < 2.4$. Events with four or more jets are rejected if each jet satisfies the criteria $E_T > 15$ GeV and $|\eta| < 2.4$. To discriminate against MJ background, the angular separation between the two highest-E_T jets must satisfy $\Delta R > 0.8$. Events that satisfy these requirements are labeled "pretagged" events.

To suppress light-flavor MJ background, at least one of the two leading-E_T jets is required to be b-tagged by the HOBIT algorithm [16], which assigns to each jet a value between 0 and 1. A jet is loosely or tightly tagged if its HOBIT-output is in a corresponding, suitably defined range. As two b quarks are present in the signal final state, events are separated into three categories based on the multiplicity and quality of the b-tagged jets: events with only one tightly tagged jet and no other tag (1 T), events with two tightly tagged jets (TT), and events with one tightly tagged jet and one loosely tagged jet (TL). Events are further classified according to the total number of jets, leading to six event subsamples. Each subsample is analyzed separately to improve the sensitivity and to help separate the events produced through s- or t-channel interactions, which are enhanced in the double- and single-tagging categories, respectively. The efficiency of the selection, taking into account all the analysis subsamples, is approximately 2.5% for t-channel and 1.7% for s-channel single top events.

All events that satisfy the above kinematic and b-tagging criteria are separated into two samples. The preselection sample consists of events that contain no identified leptons; this sample is a superset of the signal sample, defined below. The electroweak sample consists of events that contain at least one identified electron or muon; this sample is used to validate the background modeling derived for this analysis.

Most physics processes are modeled using Monte Carlo simulation programs. The single top quark samples are modeled using the POWHEG generator [17]. Backgrounds from $V + $ jets (where V represents a W or Z boson) and $W + c$ processes are modeled using ALPGEN [18]. Events from diboson (VV), $t\bar{t}$ (assuming a top-quark mass of 172.5 GeV/c^2), and Higgs bosons produced in association with a W or Z boson (VH) are simulated using PYTHIA. Parton showering is simulated in all cases using PYTHIA, using the CTEQ5L parton distribution function [19] as input to the simulations, tuned to the Tevatron underlying-event data [20]. Event modeling also includes simulation of the detector response using GEANT [21].

Two remaining backgrounds include contributions from events with falsely tagged jets ("electroweak mistags") and MJ events. The electroweak mistag samples are modeled by weighting $V + $ jets and diboson-simulated events with mistag probabilities derived from dedicated data samples [22,23]. To model the MJ background, the same data-driven method described in Ref. [24] is used: each pretagged data event is weighted by a tag-rate probability derived from a MJ-dominated data sample.

Simple requirements on the kinematic properties of the event are not sufficient to separate the single top quark signal from the background. A series of multivariate discriminants that take advantage of nontrivial variable correlations is therefore employed to optimize the suppression of MJ background and to separate the signal from the remaining backgrounds. For each of the multivariate algorithms described below, a combination of inputs is used corresponding to kinematic, angular, and event topology related quantities whose distributions are different between the background under consideration and the signal.

The dominant background in the preselection sample is MJ events. To discriminate against this background, the same $\mathrm{NN_{QCD}}$ multivariate discriminant that was developed in the $\not{E}_T b\bar{b}$ s-channel single top quark search [9] is used. All events that satisfy a minimum $\mathrm{NN_{QCD}}$ threshold requirement populate the signal region, in which the dominant backgrounds are from MJ production, $V + $ heavy-flavor-jets events, and $t\bar{t}$ events. Events that do not meet the minimal $\mathrm{NN_{QCD}}$ threshold are used to validate the background prediction with the data. From this validation, multiplicative correction factors ranging from 0.7 to 0.9 are derived for each of the 1 T, TL and TT MJ predictions so that the total predicted background

normalizations are in agreement with data. These corrections are applied to the MJ predictions in the signal region.

For all events in the signal region, two additional discriminants are developed that further exploit the differences in kinematic properties between the signal and the $V + $ jets background, and the signal and $t\bar{t}$ background processes. The first discriminant, $\mathrm{NN}_{V\mathrm{jets}}$, is trained using simulated t-channel single top quark events for the signal sample and MJ-modeled events that satisfy the requirement on $\mathrm{NN}_{\mathrm{QCD}}$, for the background sample. The second discriminant, $\mathrm{NN}_{t\bar{t}}$, is trained to separate t-channel single top quark from $t\bar{t}$ production, again using simulated t-channel single top quark events for the signal and simulated $t\bar{t}$ for the background. The values of these two discriminants are then combined in quadrature for an overall discriminant called $\mathrm{NN}_{\mathrm{sig}}^{t}$; this is analogous to the strategy adopted in Ref. [9].

The s-channel optimized $\mathrm{NN}_{\mathrm{sig}}$ discriminant as used in Ref. [9] and the $\mathrm{NN}_{\mathrm{sig}}^{t}$ discriminant of this analysis are combined to obtain an $\mathrm{NN}_{\mathrm{sig}}^{s+t}$ final discriminant, used to simultaneously separate both s- and t-channel signal processes from the remaining background. For events with $\mathrm{NN}_{\mathrm{sig}}$ output values larger than 0.6, $\mathrm{NN}_{\mathrm{sig}}^{s+t}$ is assigned to the $\mathrm{NN}_{\mathrm{sig}}$ output. For the remaining events, $\mathrm{NN}_{\mathrm{sig}}^{s+t}$ is defined as the $\mathrm{NN}_{\mathrm{sig}}^{t}$ output multiplied by 0.6. Figure 2 shows the predicted and observed distributions of the $\mathrm{NN}_{\mathrm{sig}}^{s+t}$ output variable for each of the six event subsamples used in this analysis.

Several sources of systematic uncertainty are taken into account. The dominant systematic uncertainty arises from the normalization of the $V + $ heavy-flavor background contributions. For $V + $ jets production, the heavy-flavor (HF) fraction observed in simulation is corrected based on the number of b-tagged events observed in an independent data control sample [25]. A 30% uncertainty on the $V + $ HF rate estimate is included in the fit.

Possible mismodeling in the b-tagging efficiency is taken into account by applying scale factors to the simulation so that its efficiency matches that observed in data. All scale factors are determined from data control samples, with uncertainties ranging from 8% to 16% [16]. The mistag rates are derived from the data, as are the associated 20%–30% uncertainties [16]. The uncertainties on b-tag efficiency and mistag rates have also a large impact on the final measurement.

Other uncertainties include those on the background cross sections used in the analyses. These are derived from measurements ($W + c$, 23% [26]) or from theoretical calculations ($t\bar{t}$, 3.5%; VV, 6%; and VH, 5% [27–29]). The 3%-7% uncertainty on the normalizations of the MJ background contributions is gauged by studying auxiliary data samples. All predictions whose normalizations are not constrained by data are subject to a luminosity uncertainty of 6% [30]. Furthermore, 2% uncertainties are assigned due to the efficiencies of the lepton antiselection requirement. We also assign a normalization uncertainty of 2% due to variations in the assumed parton distribution functions. To account for differences in the trigger efficiency in the data and the simulation, a 2% rate uncertainty is assigned.

Uncertainties on the jet energy scale [14] are included. The 1%–6% uncertainties on the predicted yields of signals and backgrounds are correlated with the corresponding distortions in the predicted kinematic distributions arising from jet energy scale shifts. Jet energy scale uncertainties
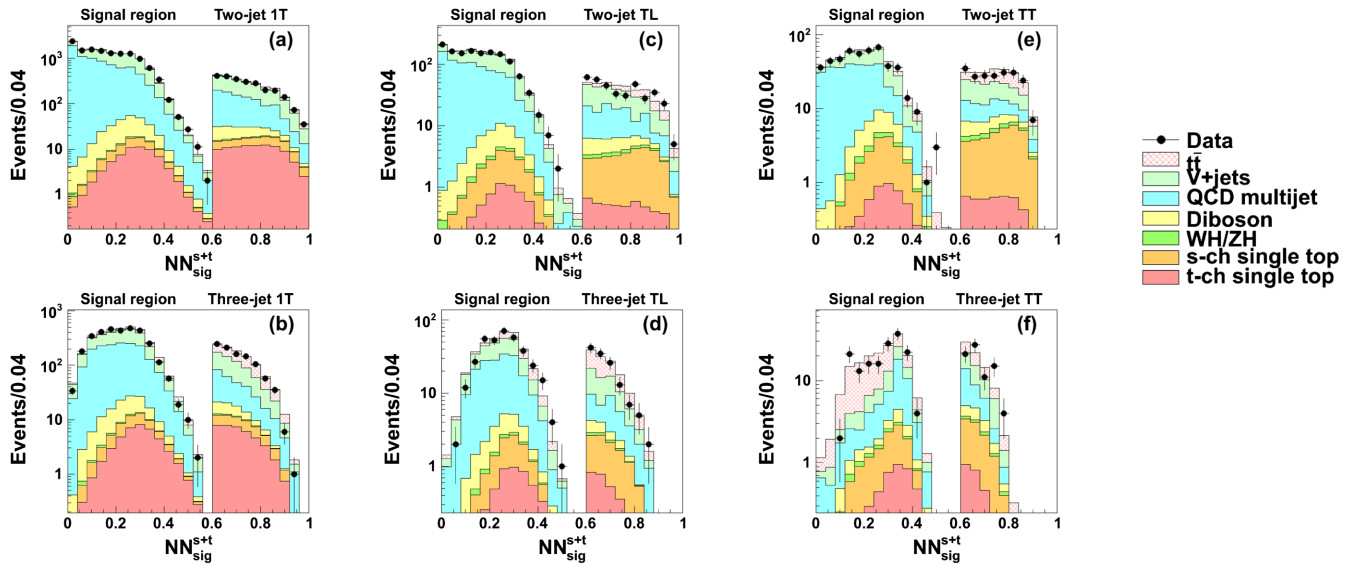

FIG. 2.   Predicted and observed $\mathrm{NN}_{\mathrm{sig}}^{s+t}$ distributions in the signal region, for the (a) 1 T two-jet, (b) 1 T three-jet, (c) TL two-jet, (d) TL three-jet, (e) TT two-jet, (f) and TT three-jet subsamples. The expected signal and background contributions are shown as filled, stacked histograms; the background is stacked on top of the signals, which are normalized to their best-fit values. The data are indicated by points with error bars.

are considered for all samples except the MJ background, which is determined entirely from data. An additional systematic uncertainty is incorporated for the MJ model, accounting for shape variations in the MJ prediction.

To measure the signal cross section, a combined likelihood is formed, which is the product of Poisson probabilities for each bin of the six NN_{sig}^{s+t} discriminants shown in Fig. 2. To account for systematic uncertainties, a Bayesian technique is used, in which each independent source of systematic uncertainty is assigned a nuisance parameter with a Gaussian prior probability density, truncated when necessary to ensure non-negative event yields. The impact of each nuisance parameter is propagated to the predictions of the signal and background yields in each bin of each histogram in the analysis. A non-negative uniform prior probability distribution is assumed for the single top quark cross section, which is extracted from its posterior probability density after integrating over all nuisance parameters. The best-fit value for the signal cross section is the one that maximizes the posterior probability density, and the uncertainties bound the smallest region which contains 68% of the integral of the posterior probability density.

Tables I and II show the event yields in the two- and three-jet subsamples, respectively, as determined from applying the measurement procedure to the six discriminants shown in Fig. 2. The observed single top quark production cross section is $\sigma_{s+t} = 3.53^{+1.25}_{-1.16}$ pb, obtained by constraining the s-/t-channel ratio to the SM prediction. This measurement is consistent with the SM predicted cross section of

TABLE I. Numbers of signal and background events in the two-jet signal region in the subsamples with exactly one tightly tagged jet (1 T), one tightly and one loosely tagged jet (TL), and two tightly tagged jets (TT). The signal and background event rates and the associated total uncertainties are the results of a fit of the predictions to the data. The backgrounds are constrained within their theoretical cross section uncertainties and uncertainties from auxiliary measurements, and the signals are left unconstrained. Signal yields for s-channel events are computed using the cross section measured constraining the t-channel contribution to the SM and the yields for t-channel events are from the cross section measurement performed by constraining the s-channel contribution to the SM.

Category	1 T	TL	TT
$t\bar{t}$	242.9 ± 24.3	84.8 ± 9.3	92.4 ± 8.4
VH	12.6 ± 1.4	6.6 ± 0.8	7.6 ± 0.8
Diboson	284.9 ± 25.6	51.3 ± 4.6	37.2 ± 3.4
$V +$ jets	6527.7 ± 1319.2	694.2 ± 113.3	220.2 ± 36.1
MJ	8328.5 ± 180.6	885.2 ± 56.7	296.8 ± 31.8
s-ch single top	86.2 ± 47.2	41.8 ± 23.0	45.9 ± 25.0
t-ch single top	160.5 ± 153.2	10.8 ± 10.3	9.2 ± 8.8
Total	15643.4 ± 1341.6	1774.8 ± 129.6	709.3 ± 55.7
Observed	15312	1743	686

TABLE II. Numbers of signal and background events in the three-jet events in the 1T, TL, and TT subsamples. See the caption of Table I for details.

Category	1 T	TL	TT
$t\bar{t}$	596.5 ± 59.6	117.5 ± 12.8	109.5 ± 9.9
VH	6.0 ± 0.7	1.9 ± 0.2	2.2 ± 0.2
Diboson	107.7 ± 9.7	15.7 ± 1.5	8.8 ± 0.8
$V +$ jets	1609.5 ± 325.5	164.5 ± 26.9	50.4 ± 8.4
MJ	1818.2 ± 48.7	187.5 ± 14.7	55.9 ± 7.7
s-ch single top	45.7 ± 25.0	15.4 ± 8.4	16.2 ± 8.9
t-ch single top	82.2 ± 78.5	7.5 ± 7.1	6.8 ± 6.5
Total	4265.7 ± 344.6	510.0 ± 35.1	249.8 ± 18.7
Observed	4198	490	237

3.15 ± 0.36 pb [4]. The magnitude of V_{tb} is extracted from the single top quark cross section posterior probability density by the relation $|V_{tb}|^2_{obs} = |V_{tb}|^2_{SM} \sigma^{s+t}_{obs}/\sigma^{s+t}_{SM}$, where variables with the subscript "SM" ("obs") correspond to the theoretical predictions (observed values) [31]. We assume $|V_{tb}|^2_{SM} = 1$ and fix the s-/t-channel ratio to the SM prediction. Including the theoretical uncertainty of the signal cross section (5.8% for s-channel, 6.2% for t-channel) [4] and assuming a uniform prior in the interval $0 < |V_{tb}|^2 < 1$, a lower bound on $|V_{tb}|$ of 0.63 is obtained at the 95% credibility level (C.L.).

Figure 3(a) shows the two-dimensional posterior probability density for the s- and t-channel cross sections, where both channels' contributions are allowed to vary independently and a uniform prior in the plane is assumed. The point that maximizes the posterior probability density is ($\sigma_s = 1.73$ pb, $\sigma_t = 0.92$ pb) and the smallest regions containing 68% and 95% of the integral of the density are indicated. To measure the t-channel cross section, we constrain the s-channel contribution to its SM prediction of 1.05 ± 0.06 pb within its uncertainty, in analogy to the procedure used in Ref. [9] to extract the s-channel single top quark production cross section. We measure the t-channel cross section to be $\sigma_t = 1.19^{+0.93}_{-0.97}$ pb, consistent with the SM prediction of 2.10 ± 0.12 pb [4]. The s-channel cross section was measured in an analysis optimized for the purpose [9], yielding $\sigma_s = 1.12^{+0.61}_{-0.57}$ pb.

These results are combined with those of the most recent CDF measurement of single top quark production in the $\ell\nu b\bar{b}$ sample [10], which measured the cross section including the tW-channel among the signal processes, yielding $\sigma_{s+t+tW} = 3.04^{+0.57}_{-0.53}$ pb, assuming a top quark mass of 172.5 GeV/c^2. The combination is achieved by collecting the inputs from the $\not{E}_T b\bar{b}$ and the $\ell\nu b\bar{b}$ analyses and taking the product of the likelihoods of both analyses and simultaneously varying the correlated uncertainties, following the procedure explained above. In the $\ell\nu b\bar{b}$ analysis, candidate events were selected by requiring
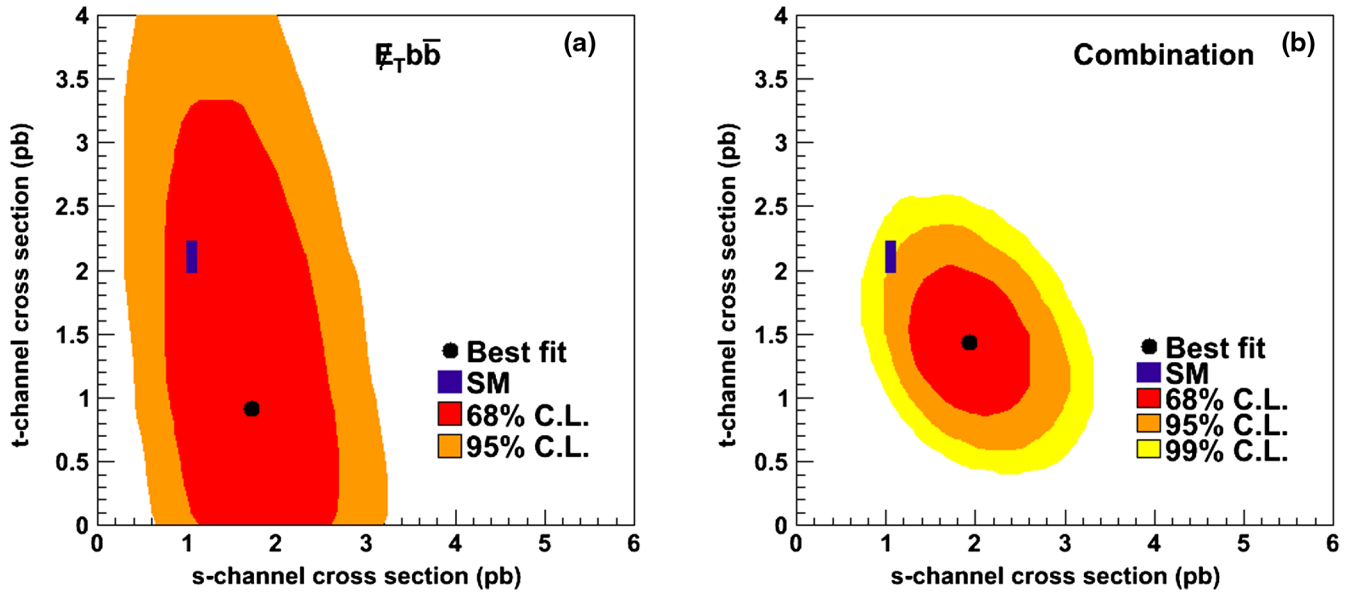
FIG. 3.   Two-dimensional posterior probability densities of the *s*- and *t*-channel cross sections for the (a) $\not{E}_T b \bar{b}$ analysis presented here, and (b) the CDF combination of the $\not{E}_T b \bar{b}$ and $\ell \nu b \bar{b}$ analysis results. Theory uncertainties are not shown.

exactly one reconstructed charged lepton (*e* or *μ*) in the final state. Hence, no such events are included in the $\not{E}_T b \bar{b}$ analysis described above. The *tW* contribution is neglected. This process is kinematically similar to $t \bar{t}$ production and its inclusion or omission from the fit does not affect the measurement of either the *s*-channel or the *t*-channel component. The uncertainties associated with the theoretical cross sections of the $t \bar{t}$, *VV*, and *VH* production processes, and those associated with the luminosity are taken as fully correlated between the two analyses.

The combined measurement results in a single top quark production cross section $\sigma_{s+t} = 3.02^{+0.49}_{-0.48}$ pb, consistent with the SM prediction. From the posterior probability density on $|V_{tb}|^2$, a 95% C.L. lower limit of $|V_{tb}| > 0.84$ is obtained. The two-dimensional posterior probability is shown in Fig. 3(b), where the *s*- and *t*-channel contributions are allowed to vary freely. The point that maximizes the posterior probability density is ($\sigma_s = 1.94$ pb, $\sigma_t = 1.44$ pb). The *t*-channel cross section, measured in the same way as for the $\not{E}_T b \bar{b}$ analysis, is $\sigma_t = 1.65^{+0.38}_{-0.36}$ pb, in agreement with the SM prediction given above. An *s*-channel cross section of $\sigma_s = 1.36^{+0.37}_{-0.32}$ pb was measured by combining the $\ell \nu b \bar{b}$ and $\not{E}_T b \bar{b}$ *s*-channel-optimized analyses as reported in Ref. [9].

In summary, an updated measurement of the single top quark production cross section $\sigma_{s+t} = 3.53^{+1.25}_{-1.16}$ pb is obtained in events with missing transverse energy and jets using the full CDF data set. This represents a relative improvement of 40% in overall precision with respect to the previous CDF $\not{E}_T b \bar{b}$ analysis [8]. The cross section for the *t*-channel-only single top quark production process as well as a 95% C.L. lower limit on $|V_{tb}|$ are also obtained. In

addition, a combination with the $\ell \nu b \bar{b}$ CDF result [10] is performed to obtain a *s* + *t* cross section measurement of $3.02^{+0.49}_{-0.48}$ pb, together with a *t*-channel-only cross section measurement of $1.65^{+0.38}_{-0.36}$ pb, which are the final and most precise measurements of these quantities from CDF. The $|V_{tb}| > 0.84$ 95% C.L. lower limit obtained from the combination is the most stringent limit on $|V_{tb}|$ from CDF. Once combined with similar results obtained by the D0 Collaboration, these results are expected to significantly improve the constraints on the parameter space of a broad class of SM extensions.

[1] V. M. Abazov *et al.* (D0 Collaboration), Phys. Rev. Lett. **103**, 092001 (2009); T. Aaltonen *et al.* (CDF Collaboration), Phys. Rev. Lett. **103**, 092002 (2009).

[2] N. Cabibbo, Phys. Rev. Lett. **10**, 531 (1963); M. Kobayashi and T. Maskawa, Prog. Theor. Phys. **49**, 652 (1973).

[3] N. Kidonakis, Phys. Rev. D **74**, 114012 (2006).

[4] N. Kidonakis, Phys. Rev. D **81**, 054028 (2010); **83**, 091503 (R) (2011).

[5] This value assumes equal contributions from singly produced top and antitop quarks.

[6] We assume a branching ratio of 100% for the standard-model $t \to W^+ b$ process.

[7] The calorimeter missing transverse energy $\vec{E}_T(\mathrm{cal})$ is defined by the sum over calorimeter towers, $\vec{E}_T(\mathrm{cal}) = -\sum_i E_T^i \hat{n}_i$, where i is a calorimeter tower number with $|\eta| < 3.6$, and $\hat{n}_i$ is a unit vector perpendicular to the beam axis and pointing at the ith calorimeter tower. The reconstructed missing transverse energy, $\vec{E}_T$, is derived by subtracting from $\vec{E}_T(\mathrm{cal})$ components of the event not registered by the calorimeter, such as jet energy adjustments. E_T [$E_T(\mathrm{cal})$] is the scalar magnitude of $\vec{E}_T$ [$\vec{E}_T(\mathrm{cal})$].

[8] T. Aaltonen *et al.* (CDF Collaboration), Phys. Rev. D **81**, 072003 (2010).

[9] T. Aaltonen *et al.* (CDF Collaboration), Phys. Rev. Lett. **112**, 231805 (2014).

[10] T. Aaltonen *et al.* (CDF Collaboration), Phys. Rev. Lett. **113**, 261804 (2014).

[11] D. Acosta *et al.* (CDF Collaboration), Phys. Rev. D **71**, 032001 (2005); **71**, 052003 (2005); **34**, 2457 (2007).

[12] We use a cylindrical coordinate system where θ is the polar angle relative to the proton beam direction at the event vertex, ϕ is the azimuthal angle about the beam axis, and pseudorapidity is defined $\eta = -\ln \tan(\theta/2)$. We define transverse energy as $E_T = E \sin\theta$ and transverse momentum as $p_T = p \sin\theta$ where E is the energy measured in the calorimeter and p is the magnitude of the momentum measured by the spectrometer.

[13] K. Potamianos, Ph.D. thesis, Purdue University; Report No. FERMILAB-THESIS-2011-34, 2011.

[14] A. Bhatti *et al.*, Nucl. Instrum. Methods Phys. Res., Sect. A **566**, 375 (2006).

[15] C. Adloff *et al.* (H1 collaboration), Z. Phys. C **74**, 221 (1997).

[16] J. Freeman, T. Junk, M. Kirby, Y. Oksuzian, T. J. Phillips, F. D. Snider, M. Trovato, J. Vizan, and W. M. Yao, Nucl. Instrum. Methods Phys. Res., Sect. A **697**, 64 (2013).

[17] S. Alioli, P. Nason, C. Oleari, and E. Re, J. High Energy Phys. 06 (2010) 043.

[18] M. L. Mangano, M. Moretti, F. Piccinini, R. Pittau, and A. D. Polosa, J. High Energy Phys. 07 (2003) 001.

[19] H. Lai *et al.*, Eur. Phys. J. C **12**, 375 (2000).

[20] T. Aaltonen *et al.* (CDF Collaboration), Phys. Rev. D **82**, 034001 (2010).

[21] GEANT, detector description and simulation tool, CERN Program Library Long Writeup Report No. W5013, 1993.

[22] D. Acosta *et al.* (CDF Collaboration), Phys. Rev. D **71**, 052003 (2005).

[23] A. Abulencia *et al.* (CDF Collaboration), Phys. Rev. D **74**, 072006 (2006).

[24] T. Aaltonen *et al.* (CDF Collaboration), Phys. Rev. D **87**, 052008 (2013).

[25] T. Aaltonen *et al.* (CDF Collaboration), Phys. Rev. D **82**, 112005 (2010).

[26] T. Aaltonen *et al.* (CDF Collaboration), Phys. Rev. Lett. **110**, 071801 (2013).

[27] P. Bärnreuther, M. Czakon, and A. Mitov, Phys. Rev. Lett. **109**, 132001 (2012).

[28] J. M. Campbell and R. K. Ellis, Phys. Rev. D **60**, 113006 (1999).

[29] J. Baglio and A. Djouadi, J. High Energy Phys. 10 (2010) 064; O. Brien, R. V. Harlander, M. Weisemann, and T. Zirke, Eur. Phys. J. C **72**, 1868 (2012).

[30] S. Klimenko, J. Konigsberg, and T. M. Liss, Report No. FERMILAB-FN-0741, 2003.

[31] This relation is robust assuming that $|V_{tb}|^2 \gg |V_{ts}|^2 + |V_{td}|^2$.